Damage identification of a 3D full scale steel–concrete composite structure with partial-strength joints at different pseudo-dynamic load levels

M. Molinari[1, *, †, ‡], A. T. Savadkoohi[1, ‡], O. S. Bursi[1, §], M. I. Friswell[2, ¶] and D. Zonta[1, ‖]

[1]*Department of Structural and Mechanical Engineering, University of Trento, via Mesiano 77, 38100 Trento, Italy*
[2]*Department of Aerospace Engineering, Queens Building, University of Bristol, Bristol BS8 1TR, U.K.*

SUMMARY

Partial-strength composite steel–concrete moment-resisting (MR) frame structures represent an open research field in seismic design from both a theoretical and an experimental standpoint. Among experimental techniques, vibration testing is a well-known and powerful technique for damage detection, localization and quantification, where actual modal parameters of a structure at different states can be determined from test data by using system identification methods. However, the identification of semi-rigid connections in framed structures is limited, and hence this paper focuses on a series of vibration experiments that were carried out on a realistic MR frame structure, following the application of pseudo-dynamic and quasi-static cyclic loadings at the European laboratory for structural assessment of the Joint Research Centre at Ispra, Italy, with the scope of understanding the structural behaviour and identifying changes in the dynamic response. From the forced vibration response, natural frequencies, damping ratios, modal displacements and rotations were extracted using the circle fitting technique. These modal parameters were used for local and global damage identification by updating a 3D finite element model of the intact structure. The identified results were then correlated with observations performed on the structure to understand further the underlying damage mechanisms. Finally, the latin hypercube sampling technique, a variant of the Monte Carlo method, was employed in order to study the sensitivity of the updated parameters of the 3D model to noise on the modal inputs. Copyright © 2009 John Wiley & Sons, Ltd.

*Correspondence to: M. Molinari, Department of Structural and Mechanical Engineering, University of Trento, via Mesiano 77, 38100 Trento, Italy.
†E-mail: marco.molinari@ing.unitn.it
‡Research Fellow.
§Professor of Structural Dynamics and Control.
¶Sir George White Professor of Aerospace Engineering.
‖Assistant Professor.

1. INTRODUCTION

Modern designs in seismic areas tend to strive for ductile behaviour of constructions [1, 2], thus providing high plastic deformations without significant reduction in resistance or the emergence of instability phenomena or collapse mechanisms. In this context, system identification and damage identification techniques constitute a promising field with widespread applications. Detecting the actual damage due to earthquakes can provide important information on the operating state and structural safety of the structures concerned. The work described herein has been performed as part of two European projects [3, 4] where a series of vibration experiments followed the application of pseudo-dynamic (PsD) and quasi-static cyclic loadings on a moment-resisting (MR) structure. The specimen was constructed and tested at the European laboratory for structural assessment of the Joint Research Centre in Ispra, and consisted of a full-scale two-storey two-bay frame with dimensions of 12.8 m by 7.4 m in plan and 7.0 m in height. Resistance to lateral seismic loads was provided by three parallel MR frames in the main direction of loading and by a bracing system in the orthogonal direction. The frames were made of composite beams and partially encased composite columns, connected by high ductile partial-strength joints designed according to the provisions of Eurocode 8 [2]. The testing programme included a sequence of PsD tests, simulating earthquakes with peak ground acceleration (PGA) scaled up to the collapse onset limit state (COLS), followed by a final cyclic test. The MR structure behaved well under seismic loading and details of the seismic design and performance can be found in [5, 6].

In recent years there has been great interest in the development of damage detection techniques for civil engineering structures [7, 8]. The significant phenomenon behind structural damage detection, localization and quantification is that some mechanical properties change due to damage. Thus in principle, by observing the variation in eigenfrequencies, damping ratios and modal shapes, it should be possible to identify any structural change as well as the global condition of a structure. Although this strategy is currently used as a mean of non-model-based damage identification [9], the application of this concept in structural engineering remains difficult for a number of reasons: (i) the complex behaviour of ductile structures that experience inelastic deformations under seismic loading; (ii) the great difficulty in exciting massive structures that are characterized by a small number of significant modes, thus reducing the amount of experimental modal quantities available; (iii) the inelasticity desired at the ends of beams in the MR frames subjected to seismic loading that determines significant changes in eigenfrequencies and damping factors but small changes in modal displacements [10]. This has motivated the application of finite element (FE) model updating to this field [11]. Through the FE model updating methodology, the differences in structural parameters, including physical and material properties and dynamic characteristics of a structure, between an FE baseline model and an updated FE model, can be obtained from the measured data. For example, Teughels *et al.* [12, 13] used modal models as well as damage functions controlled by a limited number of parameters in order to estimate the bending stiffness distribution along beam-type structures.

Wong *et al.* [14] and Ceravolo *et al.* [15] identified damage in beam-to-column joints of steel-framed structures. Both studies were successful in joint identification, although only simple beam-to-column joint models in the elastic range were considered. Chellini *et al.* [16] used modal identification in order to perform damage detection of semi-rigid partial-strength joints experiencing severe inelastic damage in the composite structure analysed in [5, 6] and characterized by low masses, low damping and complex geometry. However, the overall understanding of damage

evaluation in these structures and the issues related to the application of model updating techniques, remains largely unexplored and are the topics of this paper.

Three separate vibration test series were carried out on the test structure: first, on the intact, undamaged structure; second, after attaining the life safe limit state (LSLS); and finally, after reaching the COLS [17]. The structure was subjected to both sinusoidal and impulsive excitation and its response was recorded via three different configurations of accelerometers: one arrangement for the overall or global structural response and two sets for the analysis of interior and exterior joints, respectively. Moreover, since the structure was in a laboratory, the damage imposed was known and the bare structure could always be inspected.

The main characteristics of the prototype test structure, the test programme, the instrumentation and the main results of the modal extraction are summarized in Section 2. The 3D model of the structure and of the joints, as well as the modal updating technique based on non-linear optimization using Powell's dog leg method and relevant results are briefly described in Section 3. In the same section, both local and global damage indices of the structure are evaluated based on measured [18] and updated FE quantities. In Section 4, a variant of the Monte Carlo method, i.e. the latin hypercube sampling (LHS) technique is described [19] and used to analyse the sensitivity of the updated parameters of the 3D FE model to noise. Conclusions and perspectives are highlighted in Section 5.

2. BENCHMARK STRUCTURE, TESTS AND MODAL EXTRACTION

2.1. The benchmark structure

The full scale steel–concrete composite structure considered in the present study was constructed for the three identical MR frames shown in Figure 1, arranged at a spacing of 3.0 m. Each frame consisted of two bays of 5.0 and 7.0 m and two storeys 3.5 m in height and was reinforced with X-shaped braces in the transverse direction. Steel–concrete composite beams were formed by IPE300 steel profiles connected by full shear connection studs to a 15 cm thick concrete slab, cast on profiled sheetings. HEB260 and HEB280 partially encased steel–concrete composite columns were used as shown in Figures 1 and 2, and high-ductile partial-strength composite beam-to-column joints were designed to provide a plastic joint rotation of 35 mrad associated with a residual strength of at least 80% of their maximum value [2]. The slabs were reinforced with transversal rebars in order to activate strut and tie mechanisms between slabs and columns [2, 4]. Braconi *et al.* [5, 6] gave a complete description of the structure, including the design methods and structural performance data.

2.2. Test programme

In order to investigate the performance of the benchmark structure at different PGA levels, four PsD tests were carried out at: $0.1g$ to characterize the pseudo-elastic state; $0.25g$ for the serviceability limit state (SLS); $1.4g$ for the LSLS; and $1.8g$ for the COLS. Moreover, a final cyclic test beyond the COLS was performed. To demonstrate damage detection, three vibration tests were performed at different damage levels: Phase I for the identification of the intact structure; Phase II for the structural identification at the LSLS; Phase III for the identification beyond the COLS. Both the test programme and performance objectives are summarized in Table I.
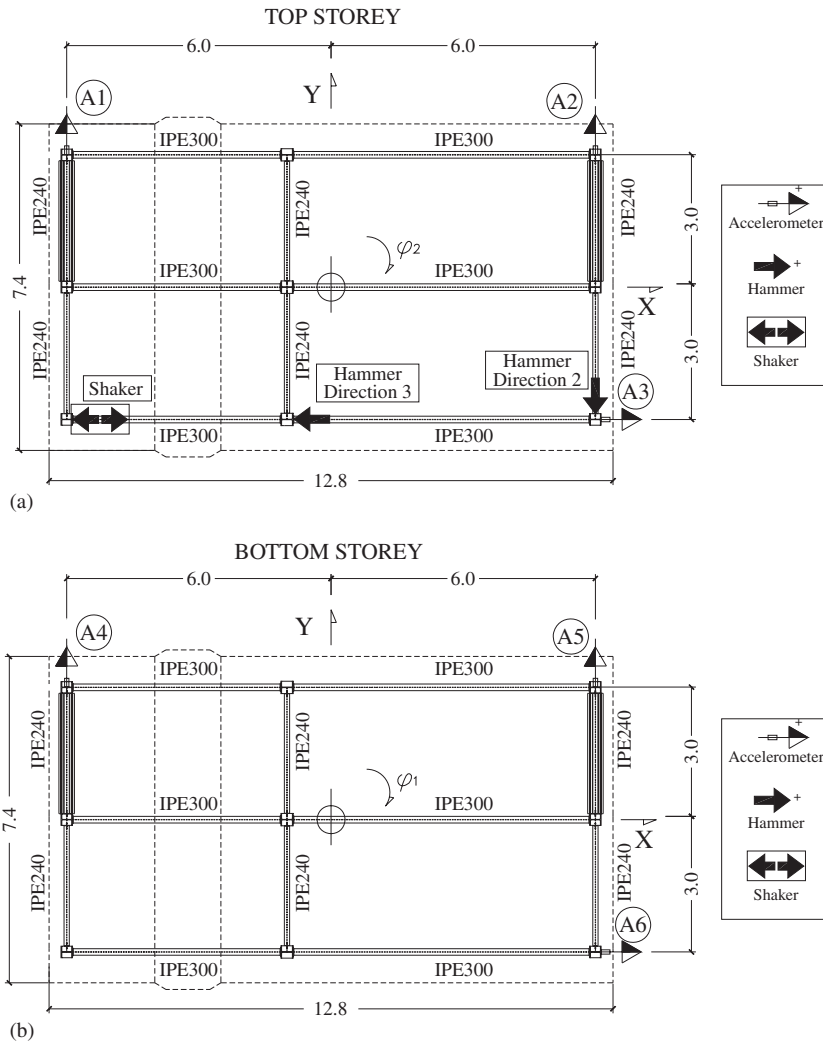
Figure 1. Location of forcing devices and global configuration A of accelerometers:
(a) location in the top storey and (b) location in the bottom storey.

In order to improve design methods on joints and to maximize the performance of the benchmark structure, preliminary tests on beam-to-column and base joints were carried out at the Universities of Pisa and Trento, Italy, respectively [20]. These results were exploited to estimate the initial stiffness values for the modal updating procedure described in Section 3.3.

2.3. Forced dynamic tests, instrumentation and modal extraction

Stepped sinusoidal tests (SST) and shock hammer tests (SHT) were performed in the three phases reported in Table I. The SSTs used an electrodynamic shaker that allowed the structure to be
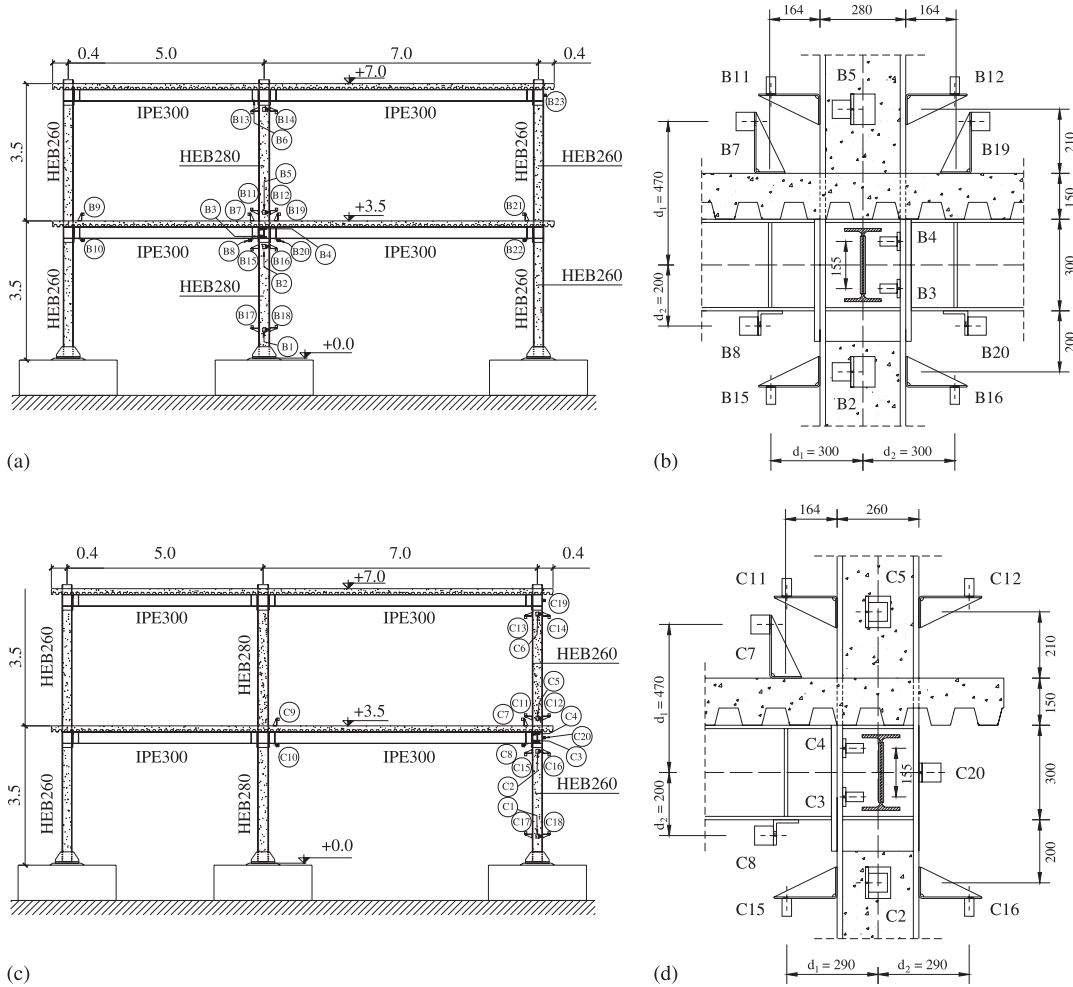
Figure 2. Local configurations of accelerometers: (a) and (b) for interior beam-to-column joints and members and (c) and (d) for exterior beam-to-column joints and members.

Table I. Summary of the test programme and performance objectives.

Test	Vibration test	PsD test PGA (g)	Performance objective
I	Phase I		Identification at the undamaged state
1		0.10	Pseudo-elastic state
2		0.25	Serviceability limit state (SLS)
3		1.40	Life safe limit state (LSLS)
II	Phase II		Identification at the LSLS
4		1.80	Collapse onset limit state (COLS)
5		Cyclic	Maximum top displacement equal to 300 mm
III	Phase III		Identification beyond the COLS

Table II. Experimental natural frequencies and damping ratios extracted from both SST and SHT tests.

	Phase I		Phase II		Phase III	
Mode	Frequency (Hz)	Damping (%)	Frequency (Hz)	Damping (%)	Frequency (Hz)	Damping (%)
1	3.36	0.57	2.38	1.27	1.95	1.44
2	5.09	0.66	4.44	0.83	4.15	0.96
3	6.92	0.70	6.24	0.67	5.70	0.68
4	10.94	0.69	8.95	0.61	8.18	0.90
5	16.48	0.49	13.95	0.30	13.72	0.59
6	22.52	0.76	19.97	0.54	19.05	0.44

excited by means of sinusoidal forces with assigned amplitude and frequency. The SHTs used an instrumented hammer that excited the structure through impulsive forces [21]. The location of the excitation forces is highlighted in Figure 1. Three different accelerometer configurations were employed in each test [17]. The global configuration A, shown in Figure 1, employed six accelerometers and allowed the overall structural dynamic behaviour to be characterized. In addition, local configurations, labelled B and C and illustrated in Figures 2(a) and (c), were used to characterize the local dynamic behaviour of interior and exterior beam-to-column joints, respectively. This was achieved by two accelerometers applied to the flanges of the columns with horizontal axes to acquire the web panel angular acceleration, as illustrated in Figures 2(b) and (d), respectively. Translational and rotational accelerations were acquired, for the instrumented sections of both beams and columns, by arranging pairs of accelerometers above and below member axes. To improve the rotation measurements, the accelerometers were well separated from the member axes. With the same set-up, some kinematic components of some base joints rotations were also monitored, as depicted in Figures 2(a) and (c).

The six lowest natural frequencies of the structure were acquired and these corresponded to two longitudinal modes (labelled 1 and 4), two transversal modes (2 and 5) and two torsional modes (3 and 6). The relevant modal properties were extracted by means of the circle-fitting technique [21]. Average values from the three configurations are listed in Table II and show the progressive reduction of natural frequencies and the corresponding increment of damping ratios with damage. Owing to the fact that low-energy dynamic tests were performed and non-structural elements were absent, the resulting damping ratios are lower than the reference values associated with elastic spectra [2], but in line with values typically extracted by vibration tests [13]. The PsD test at the SLS provided similar damping ratios [4].

3. UPDATING METHODOLOGY AND DAMAGE EVALUATION

3.1. The FE baseline model

A 3D FE model of the benchmark structure, shown in Figure 3(a), was developed in this study, and implemented and assembled in Mathematica [22]. The numerical model consists of three similar parallel frames, one of which is shown in Figure 3(b), connected through master–slave numerical constraints at each storey. Horizontal displacements within each storey and rotations around the vertical axis were constrained, whereas vertical displacements and rotations around
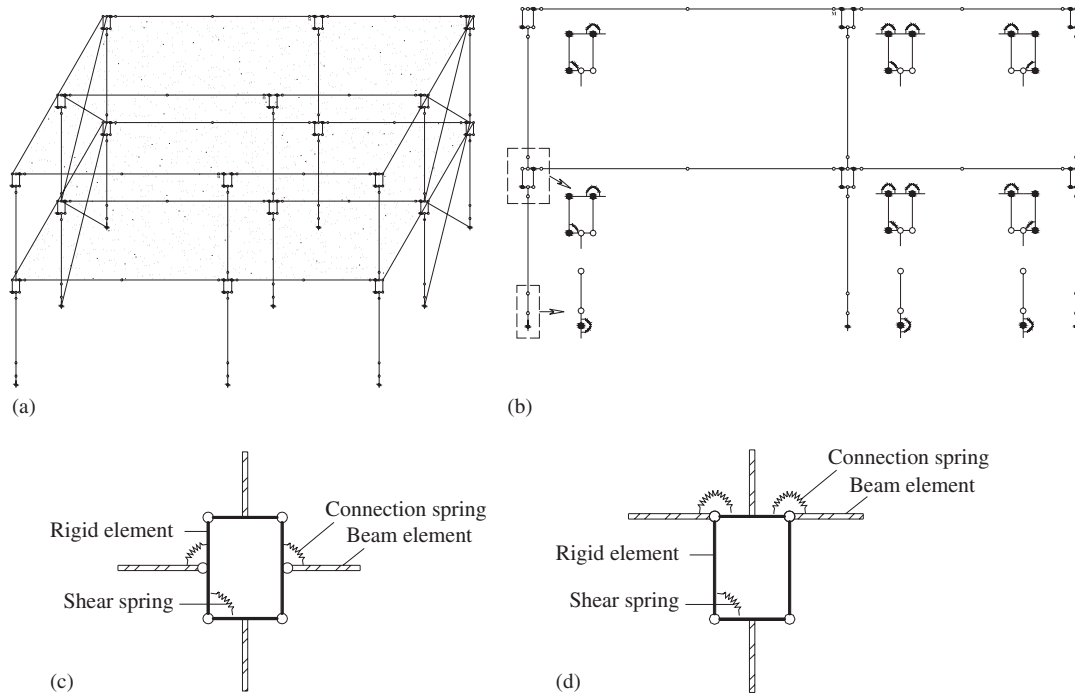
Figure 3. FE baseline models of the benchmark structure: (a) 3D model; (b) 2D model of the interior frame; (c) beam-to-column joint model; and (d) simplified beam-to-column joint model.

the horizontal axis were left free. Braces were modelled by means of truss elements; beams and columns by beam–column elements, which also accounted for shear flexibility; and base joints and beam-to-column connections by rotational springs. Beam-to-column panels were modelled by a mechanical idealization involving four rigid bars connected by pins and rotational springs, as shown in Figure 3(c). To reduce the number of degrees of freedom further, the simplified joint model illustrated in Figure 3(d) was employed.

A lumped mass model was considered with a known mass distribution. Storey masses and moments of inertia of the storeys were directly applied to the master degree of freedom, while a linear elastic behaviour for all structural elements was assumed.

3.2. FE model updating procedure

The eigensensitivity-based approach to FE model updating was employed in this study. The discrepancies between the numerical and experimental eigenvalues and eigenvectors were minimized by adjusting unknown model parameters, representing the stiffnesses of some of the structural elements within the FE model. The experimental eigenvalues, λ_X, were compared directly with the corresponding analytical eigenvalues, λ_A, and experimental eigenvectors, φ_X, were compared component by component with the corresponding analytical eigenvectors, φ_A [11]. By means of Taylor's series expansions, the differences between analytical and experimental eigenvalues and

eigenvectors of the rth mode are

$$\Delta\lambda_r = \lambda_{Xr} - \lambda_{Ar} \approx \sum_{j=1}^{N_p} \frac{\partial\lambda_{Ar}}{\partial p_j} h_{tj} \tag{1}$$

$$\Delta\boldsymbol{\varphi}_r = \boldsymbol{\varphi}_{Xr} - \boldsymbol{\varphi}_{Ar} \approx \sum_{j=1}^{N_p} \frac{\partial\boldsymbol{\varphi}_{Ar}}{\partial p_j} h_{tj} \tag{2}$$

where p_j is the jth element of the parameter vector $\mathbf{p}$ and h_{tj} is the jth element of the parameter perturbation vector $\mathbf{h}_t$ at the tth iteration. In (1) and (2), the eigenvalue and eigenvector derivatives with respect to the N_p parameters are called sensitivities and they were computed by the methods suggested by Fox and Kapoor [23] and Nelson [24], respectively. Usually eigenvalue sensitivities are one order of magnitude greater than the eigenvector sensitivities and, as a result, a numerical regularization [25] was applied in order to increase the numerical stability of the problem. Thus the left-and right-hand sides of (1) were divided by the corresponding analytical eigenvalue, λ_{Ar}. After the regularization of (1) we obtain the system of equation $\Delta_t = \mathbf{S}_t\mathbf{h}_t$, where

$$\Delta_t(\mathbf{p}) = \begin{pmatrix} \dfrac{\Delta\lambda_1}{\lambda_{A1}} \\ \Delta\boldsymbol{\varphi}_1 \\ \vdots \\ \dfrac{\Delta\lambda_m}{\lambda_{Am}} \\ \Delta\boldsymbol{\varphi}_m \end{pmatrix}, \quad S_t = \begin{bmatrix} \dfrac{1}{\lambda_{A1}}\dfrac{\partial\lambda_{A1}}{\partial p_1} & \cdots & \dfrac{1}{\lambda_{A1}}\dfrac{\partial\lambda_{A1}}{\partial p_{N_p}} \\ \dfrac{\partial\boldsymbol{\varphi}_{A1}}{\partial p_1} & \cdots & \dfrac{\partial\boldsymbol{\varphi}_{A1}}{\partial p_{N_p}} \\ \vdots & & \vdots \\ \dfrac{1}{\lambda_{Am}}\dfrac{\partial\lambda_{Am}}{\partial p_1} & \cdots & \dfrac{1}{\lambda_{Am}}\dfrac{\partial\lambda_{Am}}{\partial p_{N_p}} \\ \dfrac{\partial\boldsymbol{\varphi}_{Am}}{\partial p_1} & \cdots & \dfrac{\partial\boldsymbol{\varphi}_{Am}}{\partial p_{N_p}} \end{bmatrix}, \quad \mathbf{h}_t = \begin{pmatrix} h_{t1} \\ \vdots \\ h_{tN_p} \end{pmatrix} \tag{3}$$

The reduction in the residual between the experimental and analytical data was achieved through the minimization of the real-valued scalar objective function $F(\mathbf{p})$, that is, the non-linear function of parameters given by

$$F(\mathbf{p}) = \Delta(\mathbf{p})^{\mathrm{T}}\Delta(\mathbf{p}) \tag{4}$$

The minimization of $F(\mathbf{p})$ was carried out by Powell's dog-leg (DL) optimization technique. The DL is a hybrid method that is based on the combination of two different approaches: the Gauss–Newton (GN) and the steepest descent (SD) methods [26]. A major problem with the DL approach is the mechanism that switches between the two methods when it is appropriate, which depends on the solution at the previous step and builds a trust region where the radius changes automatically depending if the step is far or close to the minimum. Let $\mathbf{p}_t$ be the estimate of the parameter vector at the tth iteration. At the next step, the parameter vector is computed as

$$\mathbf{p}_{t+1} = \mathbf{p}_t + \mathbf{h}_{t+1} \tag{5}$$

where $\mathbf{h}_{t+1}$ is the parameter increment vector. The GN step and the SD direction are as follows:

$$\mathbf{h}_{\mathrm{GN}} = \mathbf{S}_t^{\dagger} \mathbf{\Delta}_t \tag{6}$$

$$\mathbf{h}_{\mathrm{SD}} = +\mathbf{S}_t^{\mathrm{T}} \mathbf{\Delta}_t \tag{7}$$

where $\mathbf{S}_t^{\dagger}$ is the pseudo-inverse of $\mathbf{S}_t$ [27].

During iterations, modal shifts can be experienced and owing to modelling simplifications spurious numerical modes may appear. In order to pair numerical modes with their experimental counterparts, the modal assurance criterion (MAC) [21] was systematically computed as

$$\mathrm{MAC}(\mathbf{\varphi}_{Xi}, \mathbf{\varphi}_{Aj}) = \frac{(\mathbf{\varphi}_{Xi}^{\mathrm{T}} \mathbf{\varphi}_{Aj})^2}{(\mathbf{\varphi}_{Xi}^{\mathrm{T}} \mathbf{\varphi}_{Xj})(\mathbf{\varphi}_{Ai}^{\mathrm{T}} \mathbf{\varphi}_{Aj})} \tag{8}$$

The effectiveness of this procedure depends on the quantity and type of available eigenvector components. For the frame structure, only the five lower experimental modes listed in Table II were effectively paired and retained for model updating. Moreover, only a few modal rotational components of the beams were used, because the lower modes typically involve only limited joint rotation and therefore the accuracy of the measurements is reduced.

3.3. Selection of updating parameters and local damage identification

A critical aspect of model updating is the choice of the number and type of parameters, which directly affects the shape of $F(\mathbf{p})$, its convexity and the success of the minimization procedure itself. A major issue is how to parameterize all of the unknown quantities in a convenient way, accounting for the limited experimental information and the possibility that some parameters have a small influence on the five lowest frequency experimental modes. Preliminary numerical analyses on the FE model in Figure 3(a) shows that:

  A: the bending and torsional stiffnesses of the beams and the rotational stiffnesses of the shear panels were insensitive to damage during the different Phases;
  B: the bending stiffnesses of columns in the longitudinal direction could be controlled by the same parameter;
  C: the axial stiffnesses of braces in the transverse direction could be controlled by the same parameter;
  D: the rotational stiffnesses of the beam-to-column connections and the rotational stiffnesses of base joints in the longitudinal direction appeared to be sensitive to damage in a similar way, even though the degradation mechanisms were different.

This preliminary information was complemented with a singular value decomposition analysis of the sensitivity matrix $\mathbf{S}$ [25], to define the maximum number of updating parameters that could be identified i.e. the components of $\mathbf{p}$. The number of parameters should not exceed the number of non-zero singular values of $\mathbf{S}$ for the number of reference modes employed. Because of measurement noise, a threshold has to be applied to the singular values, leading to the concept of effective rank of the problem. The FE model was updated by considering seven candidate parameters related to the stiffness of the main structural elements. Table III shows that only three significant singular values are present. Consequently, only three parameters were retained, given by

$$\mathbf{K}_j = p_j \mathbf{K}_{0j} \quad \text{for } j = 1, 2, 3 \tag{9}$$

Table III. Singular values of the sensitivity matrix **S** using seven parameters.

Singular values	Phase I	Phase II	Phase III
1	1.459	1.452	1.479
2	0.7500	0.6711	0.6242
3	0.1991	0.3049	0.3426
4	1.378E−2	8.472E−2	1.091E−2
5	2.498E−3	2.931E−3	6.037E−3
6	1.052E−3	1.392E−3	4.031E−4
7	1.394E−4	2.840E−4	2.622E−4

Table IV. Identified frequencies and percentage errors with respect to experimental values in Table II.

	Phase I		Phase II		Phase III	
Mode	Frequency (Hz)	Error (%)	Frequency (Hz)	Error (%)	Frequency (Hz)	Error (%)
1	3.36	0.1	2.33	2.2	1.96	−0.4
2	5.04	1.0	4.63	−4.2	4.20	−1.1
3	7.02	−1.5	6.44	−3.2	5.80	−1.7
4	11.51	−5.9	9.69	−8.2	8.45	−3.4
5	15.45	6.3	12.85	7.9	11.91	16.0

where $\mathbf{K}_{0j}$ defines the baseline stiffness matrix of each member. The three parameters, for $j = 1, 2, 3$, correspond to the element groups B, C and D defined above.

The concept of semi-rigid beam-to-column and base joints has been accepted in the analysis and design of steel–concrete composite structures, although determining the exact joint stiffness is still a formidable task. The initial values of Phase I for each stiffness matrix in (9) were available from the preliminary beam-to-column and base joint cyclic tests [20]. Cyclic test data were also used as initial values for the identification process in Phase III. Initial values for each element group and Phase are listed in Table VI.

Natural frequencies obtained from the model updating procedure are reported in Table IV, together with the relative error with respect to the experimental modal data are listed in Table II. The relatively large errors in the higher modes were expected, as these modes are more sensitive to modelling errors. Table V gives the MAC indices that indicate how well the FE mode shapes fit the corresponding measured ones. The identified stiffness values are summarized in Table VI and show a general reduction of stiffness values from Phase I to Phase III. As expected, stiffness reductions are more evident for beam-to-column and column base joints, where energy dissipation was sought by design [5, 6].

The variation of each member elastic stiffness can define a non-cumulative local damage index $D_{\mathrm{L}} = 1 - (k_{\mathrm{Updated}}/k_{\mathrm{Undamaged}})$, where the subscripts 'Undamaged' and 'Updated' indicate the undamaged and damaged states, as a measure of the local damage experienced by each structural element [28]. The damage values indicating the stiffness variation from Phase I to Phase II, $D_{\mathrm{L,I-II}}$, and from Phase I to Phase III, $D_{\mathrm{L,I-III}}$, are listed in Table VII. The seismic engineering literature [28] relates values of the damage index to the severity of the damage. Thus, $D < 0.1$ indicates no damage, $0.1 \leqslant D < 0.25$ corresponds to minor damage, $0.25 \leqslant D < 0.4$ indicates moderate damage and $0.4 \leqslant D < 1.0$ corresponds to severe damage. The $D_{\mathrm{L,I-II}}$ values indicate there is no damage

Table V. Diagonal MAC indices between the identified and experimental mode shapes.

Mode	Phase I	Phase II	Phase III
1	1.00	0.99	0.95
2	1.00	1.00	1.00
3	0.78	0.84	0.81
4	0.96	0.98	0.83
5	0.82	0.87	0.79

Table VI. Initial and updated element stiffnesses in the three test Phases.

Parameter	Element	Phase I		Phase II		Phase III	
		Initial	Updated	Initial	Updated	Initial	Updated
p_1	$EI_{\text{Long.,HEB260}}$ (N m^2)	3.81E7	3.80E7	3.81E7	3.76E7	3.81E7	3.68E7
	$EI_{\text{Trans.,HEB260}}$ (N m^2)	2.11E7	2.10E7	2.11E7	2.04E7	2.11E7	1.92E7
	$EJ_{t,\text{HEB260}}$ (N m^2)	1.47E7	1.45E7	1.47E7	1.43E7	1.47E7	1.37E7
	$EI_{\text{Long.,HEB280}}$ (N m^2)	4.99E7	4.98E7	4.99E7	4.93E7	4.99E7	4.81E7
	$EI_{\text{Trans,HEB280}}$ (N m^2)	2.7E7	2.77E7	2.7E7	2.69E7	2.7E7	2.53E7
	$GJ_{t,\text{HEB280}}$ (N m^2)	1.97E7	1.95E7	1.97E7	1.91E7	1.97E7	1.84E7
p_2	EA_{Braces} (N)	5.24E8	2.78E8	5.24E8	2.48E8	5.24E8	1.93E8
p_3	$K_{\phi,\text{Int.con.}}$ (N m/mrad)	1.0308	1.02E8	4.23E7	4.17E7	1.61E7	3.19E7
	$K_{\phi,\text{Ext.con.}}$ (N m/mrad)	1.08E8	9.71E7	3.83E7	3.30E7	6.24E6	1.24E7
	$K_{\phi,\text{Long.,b.j.}}$ (N m/mrad)	2.20E8	2.07E8	2.12E7	1.89E7	6.86E6	1.36E7
	$K_{\phi,\text{Trans.,b.j.}}$ (N m/mrad)	1.47E8	1.39E8	1.42E7	1.27E7	4.60E6	9.12E6

For structural elements in subscript: EI_{Long} is the flexural stiffness in the longitudinal direction; EI_{Trans} is the flexural stiffness in the transversal direction; GJ_t is the torsional stiffness; EA is the axial stiffness; $K_{\phi,\text{Int.con.}}$ and $K_{\phi,\text{Ext.con.}}$ are the rotational stiffnesses of beam-to-column connections of interior and exterior joints, respectively; $K_{\phi,\text{Long.,b.j.}}$ and $K_{\phi,\text{Trans.,b.j.}}$ are the rotational stiffnesses of base joints in the longitudinal and transversal directions, respectively.

for columns, minor damage for braces and severe damage for beam-to-column connections and base joints. After the PsD test at 1.4 PGA, visual inspection showed that the braces lost stiffness owing to light cracking of the concrete at their ends, concrete crushing happened in the composite slab close to beam-to-column joints and localized spalling of the grouting mortar from the bottom flange of base joints occurred due to the anchoring rebars yielding [6]. After the final cyclic test, see Table I, the structure was subjected to interstorey drift ratios of about 4.6% at the second storey and the ratio of the reaction force at the bottom to that at the top storey was estimated to be 0.97 by considering a modal analysis of the structure after the last PsD test. This indicates that the instrumented joints at the bottom storey, see, Figures 2(a) and (c), were also severely damaged with cracks in end plates and column flanges. Again, damage values of Table VII qualitatively reflect these phenomena.

3.4. Global damage identification

The damage state of the structure depends on both the distribution and severity of localized damage D_L. As a result, it is possible to formulate a global damage index, D_G, by combining

Table VII. Local damage indices D_L of structural elements.

Element	$D_{L,I-II}$	$D_{L,I-III}$
$EI_{Long.,HEB260}$ (Nm^2)	0.011	0.032
$EI_{Trans.,HEB260}$ (Nm^2)	0.029	0.086
$EJ_{t,HEB260}$ (Nm^2)	0.014	0.055
$EI_{Long.,HEB280}$ (Nm^2)	0.010	0.034
$EI_{Trans,HEB280}$ (Nm^2)	0.029	0.087
$GJ_{t,HEB280}$ (Nm^2)	0.021	0.056
EA_{Braces} (N)	0.110	0.310
$K_{\phi,Int.con.}$ (N m/mrad)	0.590	0.690
$K_{\phi,Ext.con.}$ (N m/mrad)	0.660	0.870
$K_{\phi,Long.,b.j.}$ (N m/mrad)	0.910	0.930
$K_{\phi,Trans.,b.j.}$ (N m/mrad)	0.910	0.930

local indices across the structure. Some authors have taken this approach (Reference [28] provides a summary), but the use of weighted averages and/or heuristic coefficients is unavoidable. The formulation of damage indices by considering global structural characteristics, such as modal parameters, is much more straightforward and attractive.

Petryna and Kratzig [18] conceived a method that uses the minimum eigenvalue of the tangent stiffness matrix of the structure to identify the onset of collapse. When the lowest eigenvalue of the tangent stiffness matrix approaches zero, the largest eigenvalue ψ_{max}^{-1} of the flexibility matrix tends to infinity. Thus the flexibility matrix, $\mathbf{G}$, was reconstructed from the experimental measurements presented in Section 2. This non-model-based method avoids the very costly procedure of model updating at the expense of a certain approximation in the results. However the flexibility matrix, $\mathbf{G}$, can be computed more reliably than its inverse $\mathbf{G}^{-1}$, which is the structural stiffness matrix. This is because the lower frequencies and corresponding mode shapes, measured from vibration tests, provide the largest contribution to the flexibility matrix. Conversely, the stiffness matrix $\mathbf{G}^{-1}$ is dominated by the higher modes, which are rarely available from tests. Thus, the flexibility matrix may be written as

$$\mathbf{G} = \boldsymbol{\varphi} \boldsymbol{\Lambda}^{-1} \boldsymbol{\varphi}^T \tag{10}$$

where $\boldsymbol{\Lambda}$ is the matrix of experimental eigenvalues and the largest eigenvalue, ψ_{max}^{-1}, can be computed by solving the eigenvalue problem

$$\mathbf{G}\boldsymbol{\Theta} = \boldsymbol{\Psi}^{-1}\mathbf{I}\boldsymbol{\Theta} \tag{11}$$

where $\boldsymbol{\Theta}$ defines the eigenvector matrix. Thus the global damage index, D_G, may be defined as

$$D_G = 1 - \frac{\psi_{max,Undamaged}^{-1}}{\psi_{max,Updated}^{-1}} \tag{12}$$

This damage index was computed based on the lower three experimental modes alone (modes 1–3 of Table II) and also on all of the six measured modes. Table VIII reports the resulting values of D_G that appear almost identical, thus showing the limited effect of the modal truncation. Moreover, since $D_G \geqslant 0.4$, the structure was severely damaged after Phase II and III, as confirmed by visual inspection.

Table VIII. Global damage indices G_L of the structure.

Method	$D_{G,I–II}$	$D_{G,I–III}$
Based on three experimental modes	0.4652	0.6274
Based on six experimental modes	0.4650	0.6274
Based on the updated flexibility matrix	0.5212	0.6669

The flexibility matrix, **G**, and its largest eigenvalue, ψ_{max}^{-1}, were also computed from the updated FE model by inverting the stiffness matrix. The corresponding values of D_G are reported in the fourth row of Table VIII and show higher damage index values. These indices may be a more realistic reflection of the damage because of the greater information involved in evaluating the stiffness matrix through modal updating. More details can be found in [29].

4. SENSITIVITY STUDY

Noise is inevitable in the real world and should be taken into account in a robust identification procedure [11]. Two types of noise are typically encountered, namely system noise owing to modelling errors; and measurement noise, owing to instrument resolution, electrical noise and environmental effects. It is evident that the presence of noise could adversely affect both the convergence process and the accuracy of the identified results. Thus, a sensitivity study should be performed on the identified FE model shown in Figure 3(d) to determine the effect of random variation in the input data on the parameter estimation. The effect will depend on the properties of the model, on the number of inputs and on the number of updating parameters chosen. Standard Monte Carlo simulations were used to investigate the properties of the estimation procedure. The LHS technique [19, 30] is a stratified sampling technique that can be applied to multiple variable problems and is used here to generate more uniform samples with equal probability and allows the reduction in the number of simulation runs.

A key aspect in the application of Monte Carlo simulation is the generation of appropriate values of the random variables that correspond to the prescribed probability distributions. This can be systematically accomplished for each variable by first generating uniformly distributed random numbers between 0 and 1, and applying an appropriate transformation to obtain the specific probability distribution. Consider a random variable X with the cumulative distribution function (CDF) $F_X(x)$ shown in Figure 4(a). At a given cumulative probability $F_X(x) = u$, the value of x will be

$$x = F_X^{-1}(u) \tag{13}$$

The LHS method selects n different values from each of the m variables $X_1, X_2, \ldots, X_m$. To produce n data samples for each variable X_i, the range of each variable is divided into n non-overlapping, equal probability intervals and one value from each interval is randomly sampled. The n values thus obtained for X_1 are paired in a random manner with the n values of X_2 and so on, until an $n \times m$ table is formed. This $n \times m$ table is the same as the $n \times m$ dimensional input vectors. For example, to generate a LHS of size $n = 5$ with m input variables, we assume that the
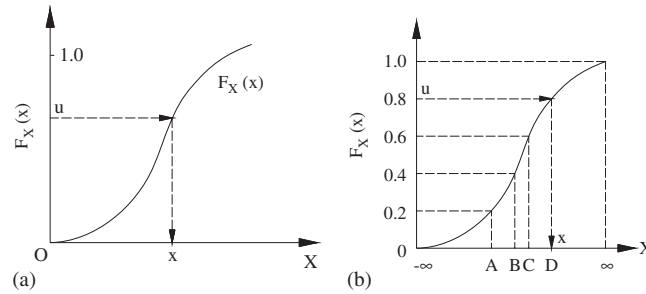
Figure 4. Generation of random variable values: (a) Monte Carlo method
and (b) latin hypercube sampling method.

first random variable X_1 has a normal distribution with mean value μ and standard deviation σ. The aforementioned procedure is illustrated in Figure 4(b) in terms of the CDF. Thus we have

$$P(-\infty \leqslant X_1 \leqslant A) = P(A \leqslant X_1 \leqslant B) = P(B \leqslant X_1 \leqslant C) = P(C \leqslant X_1 \leqslant D) = P(D \leqslant X_1 \leqslant \infty) = 0.20 \quad (14)$$

However, this ordering and pairing in the LHS technique creates an unavoidable correlation among generated data. In order to induce the desired correlation matrix between m sets of generated variable data, the restricted pairing algorithm of Iman and Conover [31] was implemented. Thus, a synthetic data set was generated that was able to reproduce the correlation structure of real data and to preserve the exact marginal distribution.

Both the system and measurement noise of the test structure were simulated through variation in the modal quantities. The normal probability distribution was used, with mean values corresponding to experimental measurements and standard deviations, σ, as follows:

(a) *eigenvalues*:

$$\sigma_\lambda = 0.0004\lambda \quad (15)$$

(b) *displacement components of eigenvectors*:

$$\sigma_{\phi_{d,i}} = 0.04 \times |\varphi_{d,\max}| + 0.04 \times |\varphi_{d,i}| \quad (16)$$

(c) *rotational components of eigenvectors*:

$$\sigma_{\phi_{r,i}} = 0.075 \times |\varphi_{r,\max}| + 0.075 \times |\varphi_{r,i}| \quad (17)$$

where λ, $\varphi_{d,i}$, $\varphi_{r,i}$, $\varphi_{d,\max}$ and $\varphi_{r,\max}$ are eigenvalues, modal displacements and rotations, and maximum values of modal displacements and rotations, respectively.

Owing to the uncertain correlation degree of the actual measurements, the analysis was repeated for each of the three phases by using both perfectly uncorrelated reference data and fully correlated reference data; the actual data are within these limits. Fifty data sets were generated for each limit

case. For example, the correlation matrix for the generated eigenvalues in Phase I, for the fully correlated data, is

$$
\begin{bmatrix}
0.999 & 0.997 & 0.998 & 0.998 & 0.998 \\
0.997 & 0.999 & 0.997 & 0.997 & 0.998 \\
0.998 & 0.997 & 0.999 & 0.999 & 0.998 \\
0.998 & 0.997 & 0.999 & 1.000 & 0.998 \\
0.998 & 0.998 & 0.998 & 0.998 & 0.999
\end{bmatrix}
\tag{18}
$$

while for the fully uncorrelated data is

$$
\begin{bmatrix}
0.999 & -0.021 & -0.071 & 0.066 & -0.019 \\
-0.021 & 1.000 & 0.065 & 0.069 & 0.000 \\
-0.071 & 0.065 & 1.000 & 0.030 & 0.084 \\
0.066 & 0.069 & 0.030 & 0.999 & -0.001 \\
-0.019 & 0.000 & 0.084 & -0.001 & 0.999
\end{bmatrix}
\tag{19}
$$

The good quality of generated data is evident. Other details can be found in [32].

Table IX shows the results of model updating for both perfectly uncorrelated and fully correlated input data. The results are reported in the form of the coefficient of variation, C_v, defined as the ratio of the standard deviation of each updated parameter in $\mathbf{p}$ to its mean value. The kernel density $\hat{f}(p)$ plot provided by the S-Plus software [33] of the updated parameters relevant to braces and connection springs for each phase are shown in Figures 5(a) and (c) for the uncorrelated input case and in Figures 5(b) and (d) for the correlated input case, respectively. The results clearly show that the updated brace stiffness has the smallest variation, compared with stiffnesses of the columns and joints in all damage phases. This implies that the braces were modelled well and that the MR structure was very sensitive to the brace stiffness in the transverse direction.

In the longitudinal direction the behaviour of the structure was mainly controlled by column flexural stiffness and by beam-to-column and base joint rotational stiffnesses. The corresponding parameters appear to be more sensitive to noise and more difficult to identify with the sensor location highlighted in Figure 2 and the FE model shown in Figure 3, because only two modes

Table IX. Coefficient of variation C_v of identified elements generated through the latin hypercube sampling method.

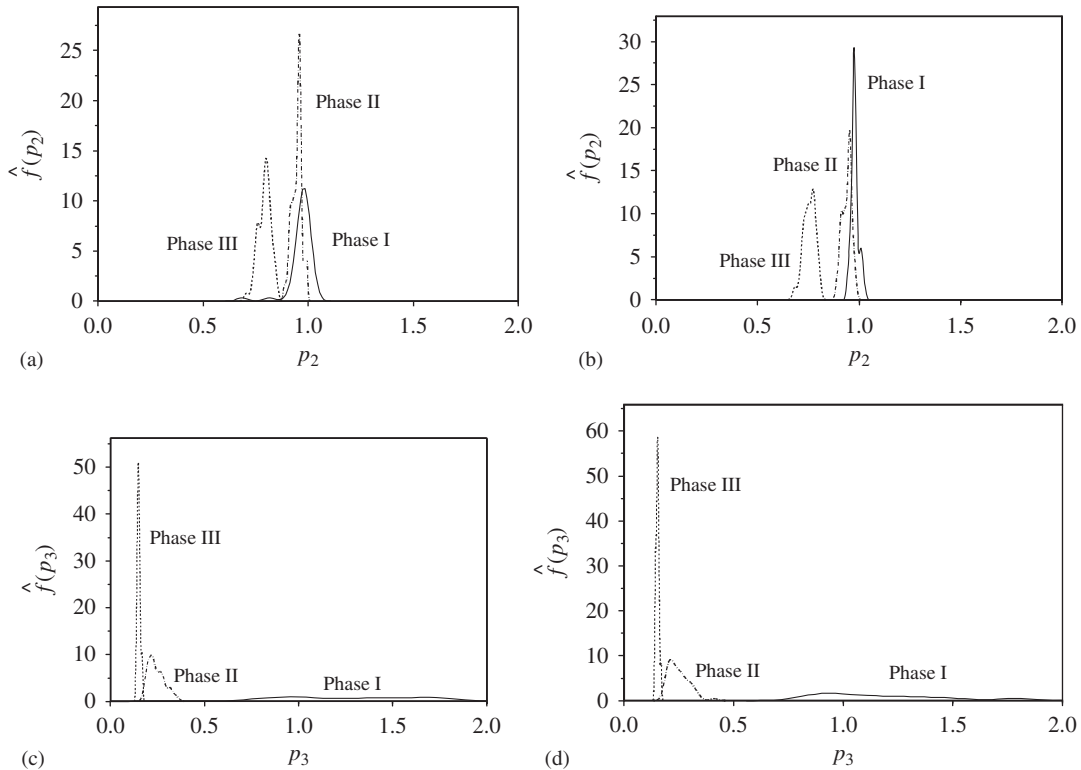| Phase	Data	C_v		
		Columns	Braces	Connections and base joints
I	Uncorrelated	0.386	0.054	0.309
	Correlated	0.216	0.018	0.246
II	Uncorrelated	0.169	0.022	0.181
	Correlated	0.186	0.025	0.191
III	Uncorrelated	0.125	0.039	0.057
	Correlated	0.184	0.039	0.046

Figure 5. Kernel density $\hat{f}(p)$ plot for updated parameters of: (a) braces with uncorrelated input data; (b) braces with correlated input data; (c) connections and base joints with uncorrelated input data; and (d) connections and base joints with correlated input data.

were measured in this direction. Furthermore, the sensitivity analysis shows that Phase I was the most sensitive to noise, mainly because the structure was elastic and undamaged. Conversely, the parameter variations in Phases II and III became smaller for columns, connections and base joint stiffnesses, for two reasons: the exploitation of reliable initial values of stiffness that were obtained from the cyclic model updating; and the greater flexibility of the structure owing to the damage caused by cyclic loading made the model updating less sensitive to noise.

5. CONCLUSIONS

An eigensensitivity-based 3D FE model updating methodology was developed in this paper for the identification of structural parameters and damage evaluation of an innovative full scale steel–concrete composite MR structure with semi-rigid and partial strength beam-to-column joints. Extensive vibration analyses were performed on the undamaged structure at two damage levels. The basic aim was to characterize the dynamic properties of the structure, damaged after realistic PsD tests at different PGAs.

Beam-to-column joints stiffnesses were identified by using an innovative beam-to-column joint model that incorporated the deformability of both beam-to-column connections and web panels. Moreover, a robust minimization algorithm based on Powell's DL method was used in the FE model updating, to assure the accurate identification of brace, column, beam-to-column and base joint stiffnesses. The updated stiffness values, eigenvalues and eigenvectors were used to compute local and global damage indices and the results were consistent with the actual damage exhibited by the structure.

In order to assess the reliability of the identified parameters, a sensitivity analysis was performed on the updated FE model by applying numerical noise onto the modal quantities. Simulations were performed by means of the LHS technique, which is a powerful variant of the Monte Carlo procedure. By considering both uncorrelated and correlated input data, it was shown that the stiffnesses of braces presented the smallest coefficient of variation compared with those of columns and joints in all damage phases, because they were able to control the sideways structural behaviour. In addition, both members and joints exhibited the lowest variation in Phase III, since more reliable initial values were obtained from a static cyclic test and because the larger flexibility of the structure owing to damage made the modal updating less sensitive to model and measurement errors.

Finally, only a small number of rotational components were retained in the model updating exercise because joint rotations were small in the lowest modes. This emphasizes the importance of the correct choice of location for accelerometers on members and joints of semi-rigid partial-strength structures. A more sophisticated 3D FE model, able to model floor flexibilities, together with the use of shakers at higher frequencies, may be required for more in-depth analysis. These enhancements will ensure the success of complex FE model updating procedures.

REFERENCES

1. AISC. *Seismic Provisions for Structural Steel Buildings*. American Institute of Steel Construction, Inc.: Chicago, IL, ANSI/AISC 341-05, 2005.
2. CEN. *Eurocode 8*: *Design of Structures for Earthquake Resistance. Part 1*: *General Rules*, *Seismic Actions and Rules for Buildings*, *EN 1998-1*. European Committee for Standardization: Brussels, Belgium, 2005.
3. Caramelli S, Salvatore W *et al.* Applicability of composite structure to sway frames. *Eur Report*, ECSC project no. 7210-PR-250, European Community, 2004.
4. Bursi OS, Caramelli S, Fabbrocino G, Molina J, Taucer F, Salvatore W, Zandonini R. 3D full scale seismic testing of a steel–concrete composite building at ELSA. *Eur Report*, Joint research Centre, European Community, 2004.
5. Braconi A, Bursi OS, Fabbrocino G, Salvatore W, Tremblay R. Seismic performance of a 3D full-scale high-ductility steel–concrete composite moment-resisting structure—part I: design and testing procedure. *Earthquake Engineering and Structural Dynamics* 2008; **37**(14):1609–1634.
6. Braconi A, Bursi OS, Fabbrocino G, Salvatore W, Taucer F, Tremblay R. Seismic performance of a 3D full-scale high-ductility steel–concrete moment-resisting structure—part II: test results and analytical validation. *Earthquake Engineering and Structural Dynamics* 2008; **37**(14):1635–1655.

7. Doebling SW, Farrar CR, Prime MB. A summary review of vibration-based damage identification methods. *The Shock and Vibration Digest* 1998; **30**(2):91–105.

8. Wang X, Hu N, Fukunaga H, Yao ZH. Structural damage identification using static test data and changes in frequency. *Engineering Structures* 2001; **23**:610–621.

9. Görel E, Link M. Damage identification using changes of eigenfrequencies and mode shapes. *Mechanical Systems and Signal Processing* 2003; **17**(1):103–110.

10. Zonta D, Elgamal AW, Fraser M, Priestly MJN. Analysis of change in dynamic properties of a frame-resistant test building. *Engineering Structures*: *The Journal of Earthquake*, *Wind and Ocean Engineering* 2008; **30**(1):183–196.

11. Friswell MI, Mottershead JE. *Finite Element Model Updating in Structural Dynamics*. Kluwer Academic Publishers: Dordrecht, 1995.

12. Teughels A, Maeck J, De Roeck G. Damage assessment by FE modal updating using damage functions. *Computers and Structures* 2002; **80**:1869–1879.

13. Teughels A, De Roeck G. Structural damage identification of the highway bridge Z24 by FE model updating. *Journal of Sound and Vibration* 2004; **278**:589–610.

14. Wong CW, Mak WH, Ko JM. System and parametric identification of flexible connections in steel framed structures. *Engineering Structures* 1995; **17**(8):581–595.

15. Ceravolo R, Demarie GV, Erlicher S. Instantaneous identification of Bouc–Wen-type hysteretic systems from seismic response data. *Key Engineering Materials* 2007; **347**:331–338.

16. Chellini G, De Roeck G, Nardini L, Salvatore W. Damage detection of a steel–concrete composite frame by a multilevel approach: experimental measurements and modal identification. *Earthquake Engineering and Structural Dynamics* 2008; **37**(15):1763–1783.

17. Bursi OS, Molina J, Salvatore W, Taucer F. *Dynamic Characterization of a 3D Full Scale Steel–Concrete Composite Building at ELSA*. European Commission, Joint Research Centre: Italy, 2004; EUR21206EN.

18. Petryna YS, Kratzig WB. Compliance-based structural damage measure and its sensitivity to uncertainties. *Computers and Structures* 2005; **83**:1113–1133.

19. McKay MD, Beckman RJ, Conover WJ. A comparison of three methods for selecting values of input variables in the analysis of output from a computer code. *Technometrics* 1979; **21**(2):239–245.

20. Salvatore W, Bursi OS, Lucchesi D. Design, testing and analysis of high ductile partial-strength steel–concrete composite beam-to-column joints. *Computers and Structures* 2005; **83**(28–30):2334–2352.

21. Ewins DJ. *Modal Testing*: *Theory*, *Practice and Application*. Research Studies Press Ltd: U.S.A., 2000.

22. Wolfram Research, Inc. *Mathematica*. Version 6.0, Champaign, IL. 2007.

23. Fox RL, Kapoor MP. Rates of change of eigenvalues and eigenvectors. *AIAA Journal* 1968; **6**(12):2426–2429.

24. Nelson RB. Simplified calculation of eigenvector derivatives. *AIAA Journal* 1976; **14**:1201–1205.

25. Jung H, Ewins DJ. Error sensitivity of the inverse eigensensitivity method for model updating. *The 10th International Modal Analysis Conference*, San Diego, CA, 3–7 February 1992; 992–998.

26. Madsen K, Nielsen HB, Tingleff O. *Methods for Non-Linear Least Square Problems*. Informatics and Mathematical Modelling, Technical University of Denmark, 2004.

27. Layton JB. Efficient direct computation of the pseudo-inverse and its gradient. *International Journal for Numerical Methods in Engineering* 1997; **40**:4211–4223.

28. Williams MS, Sexsmith RG. Seismic damage indices for concrete structures: a state-of-the-art review. *Earthquake Spectra* 1995; **11**(2):319–349.

29. Molinari M. Model updating of a steel–concrete composite mr frame structure under severe seismic loading via forced dynamic tests. *Ph.D. Thesis*, University of Trento, Italy, 2007.

30. McKay MD. Latin hypercube sampling as a tool in uncertainty analysis of computer models. *Winter Simulation Conference*, Arlington, VA, 13–16 December 1992; 557–564.

31. Iman RL, Conover WJ. A distribution-free approach to inducing rank correlation among input variables. *Communications in Statistics-Simulation and Computation-B* 1982; **11**(3):311–334.

32. Savadkoohi AT. Inverse modelling of a steel–concrete composite moment resisting structure subjected to severe cyclic loads and forced vibration tests. *Ph.D. Thesis*, University of Trento, Italy, 2008.

33. S-PLUS® (version#6.1), Insightful Corporation, Seattle, WA, 2001.